Theoretical Study of the CH_3NO_2 Unimolecular Decomposition Potential Energy Surface

Wen-Fang Hu, Tian-Jing He,* Dong-Ming Chen, and Fan-Chen Liu

Department of Chemical Physics, University of Science and Technology of China, Hefei, Anhui, 230026, P.R. China

Received: January 11, 2002; In Final Form: May 30, 2002

The complex potential energy surface for the unimolecular isomerization and dissociation of nitromethane (CH_3NO_2), including 10 CH_3NO_2 isomers, 46 interconversion transition states, and 16 major dissociation products, is probed theoretically at the G2MP2//B3LYP/6-311++G(2d,2p) level of theory. The geometries and relative energies for various stationary points are determined and are in good agreement with the available experimental values. Based on the calculated G2MP2 potential energy surface, the possible nitromethane unimolecular decomposition mechanism is discussed. It is shown that the most feasible decomposition channels for CH_3NO_2 are those that lead to $^2CH_3 + {}^2NO_2$, $^2CH_3O + {}^2NO$, $H_2C{=}O + HNO$, and $HCNO + H_2O$, respectively. Among them, $^2CH_3$ and $^2NO_2$ are produced by the direct C−N bond rupture of nitromethane, while the formation of the latter three products is initiated by CH_3NO_2 rearranging first to methyl nitrite or to aci-nitromethane. The C−N bond dissociation energy for nitromethane is calculated to be 61.9 kcal/mol, lower than the nitromethane → methyl nitrite and nitromethane → aci-nitromethane isomerization barriers by 2.7 and 2.1 kcal/mol, respectively. Our results suggest that the CH_3NO_2 isomerization pathways are kinetically disfavored in view of the relatively high activation barriers, in excess of 60 kcal/mol. The nitromethane decomposition occurs either via the C−N bond rupture or via concerted molecular eliminations.

1. Introduction

Experimental and theoretical investigations concerning the properties and reactions of nitro-containing compounds have been carried out extensively[1−9] for the significant role they play in propellant ignition, combustion, and atmosphere pollution. Information on their decomposition mechanism and kinetics is critical for understanding their extremely complex reactions in the atmosphere.

Nitromethane (NM) is the simplest organic−nitro compound as well as an important prototypical energetic material. Numerous studies have been performed on its photo and thermal chemistry.[1,10−27] The ultraviolet adsorption spectrum of NM is found to consist of a weak band at around 270 nm and a strong band at around 198 nm.[28] The dynamics of NM photodissociation following excitation in either of these adsorption regions has been actively studied for many years,[18,29−34] yet the mechanism is not completely understood. The seemingly direct gas-phase thermal decomposition of NM indicates great complexity from the competition among the various energetically allowed decay channels.[16,35−37] Several authors[38−40] in their studies of the thermal decomposition of NM identified the formation of nitric oxide, nitrous oxide, carbon monoxide, carbon dioxide, methane, ethane, ethylene, water, hydrogen cyanide, and formaldehyde. Previous experimental and theoretical investigations on NM also encompass such aspects as the bimolecular[41,42] decomposition pathways, the mechanism of sensitization toward detonation in shocked NM,[43,44] the Raman and UV−vis adsorption spectra as well as the shock-induced decomposition of liquid NM,[45,46] the multiconfigurational nature of the ground state,[47] the ground and excited-state potential energy curves for NM dissociation,[26,27] and so on.

* Corresponding author: Fax: +86-551-3603388. E-mail: tj16@ustc.edu.cn.

Conflicting views exist about the decomposition mechanism of NM, even about that in the initial reaction stage. The primary photodissociation process is generally regarded to be rupture of the C−N bond to yield a methyl radical and nitrogen dioxide.[31−34]

$$CH_3NO_2 + h\nu \rightarrow CH_3 + NO_2 \quad (1)$$

A concerted molecular elimination[48] (eq 2) and oxygen atom elimination[49] (eq 3) were also suggested to be involved in the primary processes.

$$CH_3NO_2 + h\nu \rightarrow H_2C{=}O + HNO \quad (2)$$

$$CH_3NO_2 + h\nu \rightarrow CH_3NO + O \quad (3)$$

Investigations on the pyrolysis of NM have been carried out for decades, yet the chemical mechanism of the reaction is not very clear. Briefly, the results of these studies are as follows. By recording the pressure increase at constant volume during the thermolysis of NM, Taylor et al.[38] detected the production of a large amount of nitric oxide. They postulated that unimolecular N−O cleavage (eq 4) takes the role of the rate-determining step and predicted an activation barrier of 61 000 calories.

$$CH_3NO_2 \rightarrow CH_3NO + O \quad (4)$$

Using the same method, Cottrell et al.[39] suggested the following reaction sequence, in which the possibility of O atom elimination (eq 4) was excluded in view of their estimated N−O

10.1021/jp020070n CCC: $22.00
Published on Web 07/12/2002

bond energy of more than 73 kcal:

$$CH_3NO_2 \rightarrow CH_3 + NO_2 \quad (5)$$

$$CH_3 + CH_3NO_2 \rightarrow CH_4 + CH_2NO_2 \quad (6)$$

$$CH_2NO_2 + NO_2 \rightarrow CH_2O + NO + NO_2 \quad (7)$$

$$CH_2O + NO_2 \rightarrow CO + NO + H_2O, \text{ etc} \quad (8)$$

$$CH_3 + CH_3 \rightarrow C_2H_6 \quad (9)$$

The decomposition experiment at higher pressure ranges by Mueller[40] detected the formation of large quantities of hydrogen cyanide. Then the N−O (eq 4) and C−N (eq 5) breakages were proposed to occur in competition at the initial reaction stage. NM isomerization to methyl nitrite, which will decompose to a methoxyl radical and nitric oxide (eq 10), was also indicated to compete with C−N bond rupture by the infrared multiphoton dissociation (IRMPD) experiment of Wodtke et al.[10]

$$CH_3NO_2 \rightarrow CH_3ONO \rightarrow CH_3O + NO \quad (10)$$

Using RRKM theory to fit the experimental results, they predicted a 55.5 kcal/mol nitro-nitrite isomerization barrier, which is slightly lower than the C−N bond dissociation energy (BDE, 60.1 kcal/mol). Theoretically, Dewar et al.[1] performed MINDO/3 calculations on the thermolysis of NM. They predicted the respective barriers for NM isomerization to methyl nitrite and methyl nitrite decomposition to formaldehyde plus nitroxyl to be 47.0 and 32.4 kcal/mol. They concluded that NM decomposes most easily by first rearranging to methyl nitrite. While on the MP2/6-31G*+ZPC potential energy surface by Mckee,[23] concerted rearrangement pathways have barrier heights much higher than fragmentation reactions and are supposed not to occur on the CH_3NO_2 surface.

From the discussion above, we can see that although NM is such a well-studied system, some uncertainties still exist concerning its decomposition mechanism. Therefore, a systematic exploration on the NM potential energy surface is needed. The present work is undertaken to investigate the detailed potential energy surface of NM unimolecular isomerization and decomposition at the G2MP2//B3LYP/6-311++G(2d,2p) level of theory. Based on the calculated results, the possible CH_3-NO_2 dissociation mechanism is suggested.

2. Computational Details

Previous studies have shown that the hybrid density functional theory (DFT) methods based on Becke's three-parameter functional can excellently reproduce experimental results of the geometry, dipole moment, and IR frequencies for nitromethane.[50] The obtained energy differences between the triplet and singlet NM are also in good agreement with the MCSCF value. In this work Becke's three-parameter nonlocal exchange functional[51] with Lee, Yang, and Parr's nonlocal correlation functional[52] (B3LYP) method was employed to optimize the geometries of all reactants (IS), intermediates (IM), transition states (TS) and products using the 6-311++G(2d,2p) basis set. The nature of these points and their zero-point vibration energies (ZPE, scaled by a factor of 0.96[53]) are determined from the frequency calculations at the same theory level. The optimized structures on the potential energy surface are characterized as transition states if only one imaginary frequency exists, or as minima if all nonzero frequencies are real. Intrinsic reaction coordinate (IRC) calculations are carried out using smaller basis sets to make sure the transition states connect the expected stationary points on the energy surface. Finally G2MP2 theory[54] is employed to calculate the potential energy surface (PES) for NM decomposition. The single-point energies are obtained by using QCISD(T)/6-311G(d,p), UMP2/6-311+G(3df,2p), and UMP2/6-311G(d,p) at the optimized geometries, then the G2MP2 energy is given as

$$E[\text{G2MP2}] = E[\text{QCISD(T)/6-311G(d,p)}] + E[\text{UMP2/6-311+G(3df,2p)}] - E[\text{UMP2/6-311G(d,p)}] + \text{HLC} + \text{ZPE}$$

where HLC (high-level correction) $= -0.00019n\alpha - 0.00481n\beta$, with $n\alpha$ and $n\beta$ being the numbers of α and β valence electrons, respectively. Unless otherwise specified, the G2MP2 relative energies (in kcal/mol) are used in the following discussions, by taking the eclipsed NM (IS1a) as zero for reference. All calculations are performed with the Gaussian 98 package.[55]

3. Results and Discussion

Roughly six distinct decomposition pathways (A−F) for nitromethane are investigated. The structures and optimized geometrical parameters associated with the critical points involved are depicted in Figure S1 of the Supporting Information. The G2MP2 relative energies and zero-point vibration energies calculated at the B3LYP level of theory are presented in Table 1. Based on our G2MP2 relative energies, Figures2 and 3 plot the potential energy diagram for nitromethane unimolecular decomposition and rearrangement.

3.1. Conformational Surface. *IS1, CH_3NO_2*. The energy discrepancy between the two conformations of NM, i.e., the eclipsed CH_3NO_2 (IS1a) and the staggered CH_3NO_2 (IS1b), is extremely small. The observed rotational barrier is only 0.0061 kcal/mol,[12] with IS1b being slightly favored. The internal rotation with a barrier height of such magnitude, which is within the error of most present computational methods, can be observed only at low temperatures. So our calculated value of 0.03 kcal/mol is not considered to be reliable.

IS2, CH_3ONO. Two orientations of the nitrite group in the methyl nitrite structure are involved, i.e., the cis-staggered CH_3-ONO IS2a, and the trans-eclipsed CH_3ONO IS2b. The energy difference is determined to be 0.8 kcal/mol, with IS2a being slightly favored. By surmounting an activation barrier of 11.2 kcal/mol (TS11), IS2b may transform into the cis-staggered IS2a. For more detailed analysis of the conformational surface for methyl nitrite, please refer to ref 23.

IS3, $CH_2N(O)OH$. The planar *cis*-$CH_2N(O)OH$, IS3a, where 'cis' denotes the relative location of the hydroxyl group and N−O* bond, is located 14.7 kcal/mol above NM on the PES. Two resonance structures can be depicted of IS3a, as illustrated in Figure 1. The resonance effect is reflected in the IS3a structure by a much shorter N−O* bond (1.239 Å), as compared to the usual N−O single bond. The C_1 symmetrical IS3b, 6.7 kcal/mol above IS3a, is also found as a local minimum on the PES. According to the IRC calculation, IS3b may transform into IS3a via transition state TS12. TS12 has a small imaginary frequency of 157.7 cm^{-1} and is energetically very close to IS3b, indicating that IS3b is kinetically rather unstable with respect to conversion to IS3a.

IS4, $CH_2(OH)NO$. The C_s symmetrical *cis,cis*-$CH_2(OH)NO$, IS4a, where the first 'cis' refers to the relative location of hydroxyl and C−N bond, the second one that of C−O and N−O bonds, is energetically 5.1 kcal/mol lower than NM. Mckee[23] reported the *cis,cis*-$CH_2(OH)NO$ (compound 12 in his work)

TABLE 1: Zero-Point Vibration Energies (ZPE, in kcal/mol), Entropy *S* Values (in kcal mol^{-1} K^{-1}) at 298.15 K, and Relative Energies (RE, in kcal/mol) of the Reactant, Isomers, Intermediates, Dissociation Products, and Transition States Calculated at the B3LYP/6-311++G(2d,2p) and G2MP2 Levels

species	B3LYP/6-311++G(2d,2p) ZPE	B3LYP/6-311++G(2d,2p) S	G2MP2 RE	expt/ other results	species	B3LYP/6-311++G(2d,2p) ZPE	B3LYP/6-311++G(2d,2p) S	G2MP2 RE	expt/ other results
IS1a	31.1665	71.210	0.		TS1[a]	28.3103	69.355	64.6	55.5(ref 10) 73.53(ref 23)
IS1b	31.1835	69.578	0.03	−0.006[exp.](ref 12)	TS2	25.8099	67.578	43.0	
IS2a	30.2365	67.110	1.2	3.52[exp.](ref 59)	TS3[b]	25.7296	78.214	59.3	
IS2b	30.0373	68.727	2.0	5.62(ref 23)	TS4	27.7180	64.007	64.0	
IS3a	30.7839	65.584	14.7	21.84(ref 23)	TS5	23.2770	68.737	102.2	
IS3b	30.3080	67.651	21.4		TS6	26.0291	69.709	62.9	
IS4a	30.4467	66.502	−5.1	1.66 (5.99, ref 23) see text	TS7 + ^{3}O	23.5970	95.887	154.1	
IS4b	30.2039	69.401	−2.0		TS8 + ^{3}O	27.0278	96.193	90.9	
IS5	30.3391	65.530	28.9	31.21(ref 23)	TS9 + ^{3}O	22.5404	98.441	139.6	
IS6a	29.7881	68.247	55.3		TS10 + H_2	20.6398	93.828	96.3	
IS6b	29.6868	67.661	53.3		TS11	29.3683	66.552	13.2	
IS6c	29.2265	68.896	57.5		TS12[b]	30.1517	64.343	21.2	
IS7a	31.3307	66.754	−25.4		TS13 + H_2	21.0256	94.940	19.2	
IS7b	31.3256	66.454	−26.7		TS14 + ^{2}NO	22.8977	105.501	75.3	
IS8	31.4235	66.755	7.0		TS15[b]	25.1183	68.692	47.4	
IS9a	30.8093	66.931	−16.5		TS16 + ^{2}NO	20.3005	107.687	67.7	
IS9b	31.1377	66.892	−21.9		TS17	28.2519	67.214	77.6	
IS9c	31.4221	66.677	−19.6		TS18	28.8965	65.755	76.0	
IS10a	31.7776	64.920	−14.9		TS19	27.1573	66.535	75.6	
IS10b	31.4905	66.389	−4.0		TS20[b]	25.8098	67.571	43.0	
IS10c	30.9779	67.118	−1.5		TS21[b]	27.2894	67.329	60.8	
IM1	30.0311	68.750	2.0		TS22[b]	27.6565	65.235	36.3	
IM2	29.0862	70.835	20.2		TS23	28.7650	64.515	95.1	
$^2CH_3$ + $^2NO_2$	24.1128	103.770	61.9	60.1[exp.](ref 59) 58.5[exp.](ref 60)	TS24	27.8387	64.133	27.2	
H_2C=O + HNO	25.3922	104.928	14.9	15.7[exp.](ref 59)	TS25	26.7317	65.711	54.5	
H_2C=O + HON	25.0854	104.947	57.4		TS26	30.3625	65.468	1.5	
$^2CH_3O$ + ^2NO	25.4833	105.680	45.0	43.0[exp.](ref 59)	TS27[b]	27.9608	64.517	80.0	
^2H + $^2CH_2NO_2$	22.0524	94.364	103.3	102.0(ref 21) 107.5[exp.](ref 61)	TS28	27.2952	66.861	102.5	
^3O + CH_3NO	27.0503	98.372	94.7	93.3(ref 21)	TS29	26.4547	67.959	29.9	
^3O + *cis*-CH_2NOH	27.5873	96.830	88.1		TS30[b]	28.1516	67.189	29.4	
^3O + *trans*-CH_2NOH	27.9169	96.941	83.2		TS31	27.8372	66.433	16.6	
^3O + HCN + H_2O	23.6161	129.619	51.0		TS32	29.2434	63.552	−13.7	
^2NO + $^2CH_2OH$	26.1019	106.602	36.4		TS33	27.2777	69.265	35.6	
^2H + H_2C=O + ^2NO	19.4495	128.635	62.9		TS34	27.1756	68.181	34.2	
HCNO + H_2O	25.5853	101.651	−0.1		TS35[b]	24.1568	67.116	57.7	
HNCO + H_2O	26.7946	102.034	−68.5	−69.9[exp.](ref 59)	TS36[b]	27.2676	65.159	43.3	
HOCN + H_2O	26.9455	102.759	−43.1		TS37	27.1370	66.118	40.1	
HONC + H_2O	26.1530	104.492	14.7		TS38	26.0171	69.942	60.2	
cyclic NC(H)O + H_2O	25.8642	103.718	15.6		TS39	25.9539	74.271	47.1	
CH_2 + HONO	23.0928	104.500	99.3	95.6[exp.](ref 59)	TS40[b]	28.1194	65.241	53.8	
HCN + H_2O_2	26.8991	102.377	17.8		TS41	27.9193	65.339	54.0	
H_2 + $HCNO_2$	21.0767	95.396	96.6		TS42	29.5562	65.410	55.5	
H_2 + nonplanar HC(O)NO	21.3258	98.318	19.3		TS43	29.1598	66.302	58.5	
H_2 + planar HC(O)NO	21.4776	97.536	16.5		TS44	30.7481	65.377	−10.6	
2HCO + 2HNOH	Q	109.363	50.9		TS45	30.2279	66.125	−11.6	
					TS46	30.9381	64.733	−2.9	

[a] Unless otherwise noted, IRC calculations of the reactions associated with these transition states are performed at the B3LYP/6-31G(d,p) level. [b] IRC calculations performed at the B3LYP/6-311G(d,p) level.

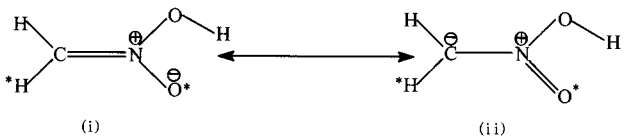

Figure 1. Resonance structures for planar *cis*-$CH_2N(O)OH$.

as 5.99 kcal/mol above the eclipsed CH_3NO_2 (compound 2 in his work). However, from the description he presented later, we conclude that the *cis*,*cis*-$CH_2(OH)NO$ he depicted in Figure 1 as compound 12 is actually compound 11 in Tables 1 and 2. Therefore, the energy difference estimated by Mckee is actually 1.66 kcal/mol, with the *cis*,*cis*-$CH_2(OH)NO$ being higher in energy. Another C_1 symmetrical conformer of $CH_2(OH)NO$, IS4b, is located 2.0 kcal/mol below NM by our calculation. The transformation between IS4b and IS4a goes through transition state TS26, 3.5 kcal/mol above IS4b.

IS5, H_2(CON)OH. Owing to the three-membered CON ring in its structure, IS5 has a relatively high total energy, about 28.9 kcal/mol above NM. The suggested H_2(CON)OH fragmentation into H_2C=O + HNO[23] is not realized in this work. On the contrary, we find that H_2(CON)OH has barriers to isomerizations into $CH_2N(O)OH$, $CH_2(OH)NO$, and HC(O)N(H)OH in excess of 45 kcal/mol.

IS6, $HCN(OH)_2$. $HCN(OH)_2$ is the highest-energy isomer studied. One planar conformer, IS6a, and two C_1 symmetry conformers, IS6b and IS6c, are optimized. The *cis*,*trans*-$HCN(OH)_2$, IS6a, where 'cis' denotes the relative location of O*−H and C−N bonds, and 'trans' that of O−H and N−O* bonds, is located 55.3 kcal/mol above NM on the PES. Via transition states TS42 and TS43, IS6a may transform into its nonplanar conformers IS6b and IS6c. The respective IS6a → IS6b, IS6b → IS6a, IS6a → IS6c, and IS6c → IS6a barriers are 0.2, 2.2,

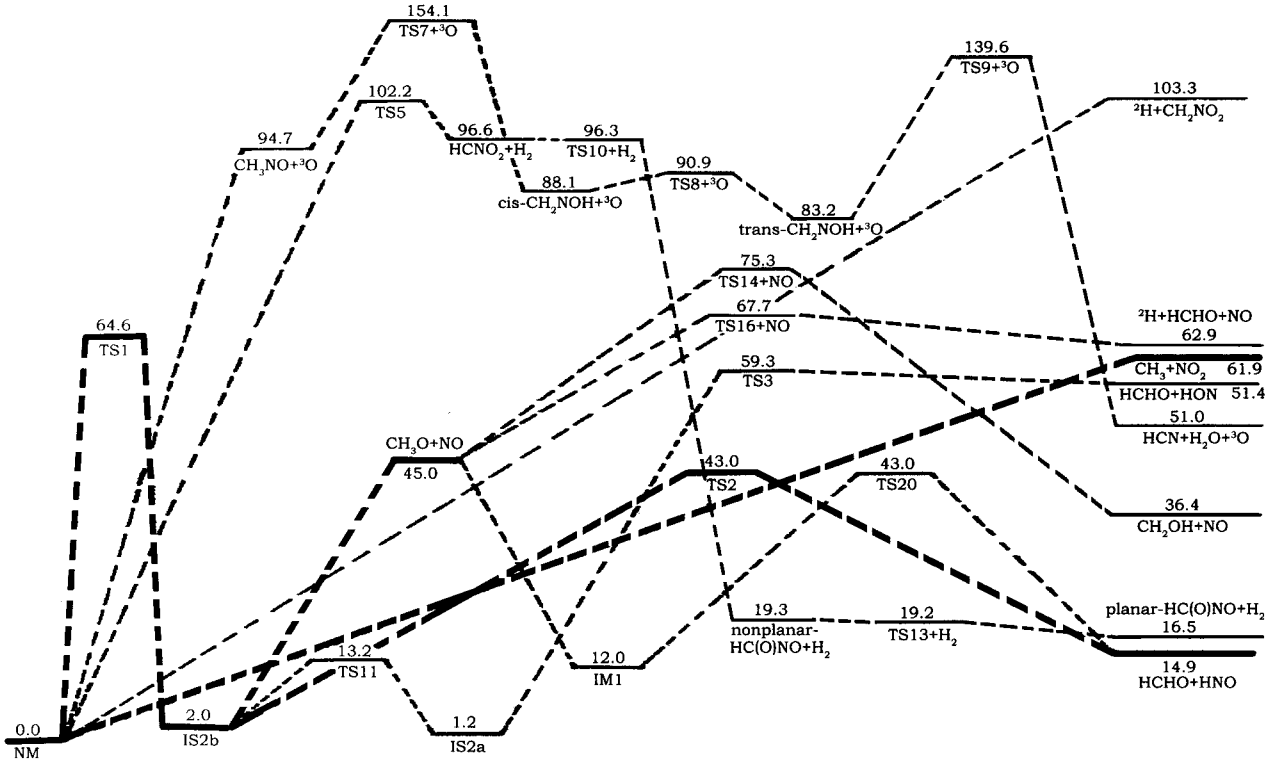

Figure 2. G2MP2 potential energy diagram for CH_3NO_3. Decomposition pathways A, B, C, D, and F. The most feasible decomposition routes are delineated in bold lines. The energies are in kcal/mol.

3.2, and 1.0 kcal/mol at the G2MP2 level. The very low IS6c → IS6a and IS6a → IS6b barriers indicate that IS6c is kinetically rather unstable for conversion to IS6a, while the latter is kinetically rather unstable for conversion to IS6b.

IS7, HC(O)N(H)OH. Two C_1 symmetry conformers of HC(O)N(H)OH, IS7a and IS7b, are the lowest in energy located on the NM conformational surface reported in this paper. In the optimized structure of IS7a, the N−O and C−O* bonds are approximately in a trans location, the O−N−C−O* dihedral angle being 160.0°, while in IS7b, they are in an approximate cis location, the O−N−C−O* dihedral angle being −10.0°. Energetically, IS7a is higher than IS7b by 1.3 kcal/mol. Going through transition state TS44, IS7a may rearrange to IS7b. The energy barrier is 14.8 kcal/mol relative to IS7a.

IS8, HC(O)N(O)H$_2$. A N → O coordination bond is characteristic of the bonding of HC(O)N(O)H_2. The charge distribution analysis shows that the nitrogen atom carries positive atomic charges, while the O atom bonded to it carries the largest negative charges in HC(O)N(O)H_2. The N−O bond length is found to be 1.378 Å at the B3LYP level. IS8 is thermodynamically less stable than NM by 7.0 kcal/mol.

IS9, HC(OH)NOH. All three conformations studied here are planar in structure. The two trans conformers of HC(OH)NOH, IS9a and IS9b, where 'trans' denotes the relative location of C−O and N−O bonds, are lower in energy than NM by 16.5 and 21.9 kcal/mol, respectively. Their interconversion is comparatively easy in view of the 4.9 kcal/mol barrier to IS9a → IS9b (TS45). IS9c, 19.6 kcal/mol below NM, is the only cis conformer studied of HC(OH)NOH. The interconversion between the trans and the cis conformations of HC(OH)NOH is forbidden because the internal rotation about the C−N bond will destroy C−N π bond formed in HC(OH)NOH.

IS10, HC(OH)N(O)H. As in the case of planar *cis*-CH_2N(O)OH (IS3a), two resonance structures just like those illustrated in Figure 1 can be depicted, respectively, of all three planar conformers of HC(OH)N(O)H, IS10a, IS10b, and IS10c. The respective N−O bond lengths in IS10a, IS10b, and IS10c are 1.305, 1.278, and 1.288 Å. The two cis conformers, IS10a and IS10b, are energetically 14.9 and 4.0 kcal/mol lower than NM. It is shown that IS10b is kinetically unstable with respect to conversion to IS10a. The energy barrier (TS46) is only 1.1 kcal/mol. IS10c, 1.5 kcal/mol below NM, is the trans conformer studied of HC(OH)N(O)H. Likewise, the transformation between the cis and the trans conformations of HC(OH)N(O)H is forbidden.

IS1 → IS2 Isomerization. Nitro-nitrite rearrangement is suggested to compete with C−N bond rupture in the initial steps of NM decomposition.[10] Determination of the structure and energy of the transition state has always been a focus of great disagreement. A tight transition state was located using the MINDO/3 method,[1] with C−N and C−O bond lengths being 1.516 and 1.584 Å, respectively, and an activation barrier of 47.0 kcal/mol, about 13 kcal/mol lower than the C−N BDE. Mckee[23] reported (at SCF level) a transition state of C−N and C−O bond lengths on the order of 2 Å and a barrier (73.5 kcal/mol) much higher than the C−N BDE. By constructing three model potential energy surfaces, the classical trajectory calculations of Rice and Thompson[21] found the third potential energy surface (PES3), which has similar C−N and C−O bond lengths to those in ref 23 but a significantly lower barrier (47.6 kcal/mol), in best agreement with the experimental branching ratio.[10] Note that PES3 is purely an empirical model whose dynamics could reasonably reproduce the experimental branching ratio. Thus it might not be totally reliable in characterizing the nature of the transition state. Besides, a loose transition state was reported by Saxon et al.[25] at the MCSCF/CI level, with the bond lengths about 3.5 Å and an energy barrier a little below the C−N BDE. If such a loose transition state does exist, it's more likely that the rearrangement occurs via a decomposition−recombination mechanism. However, there are no reliable

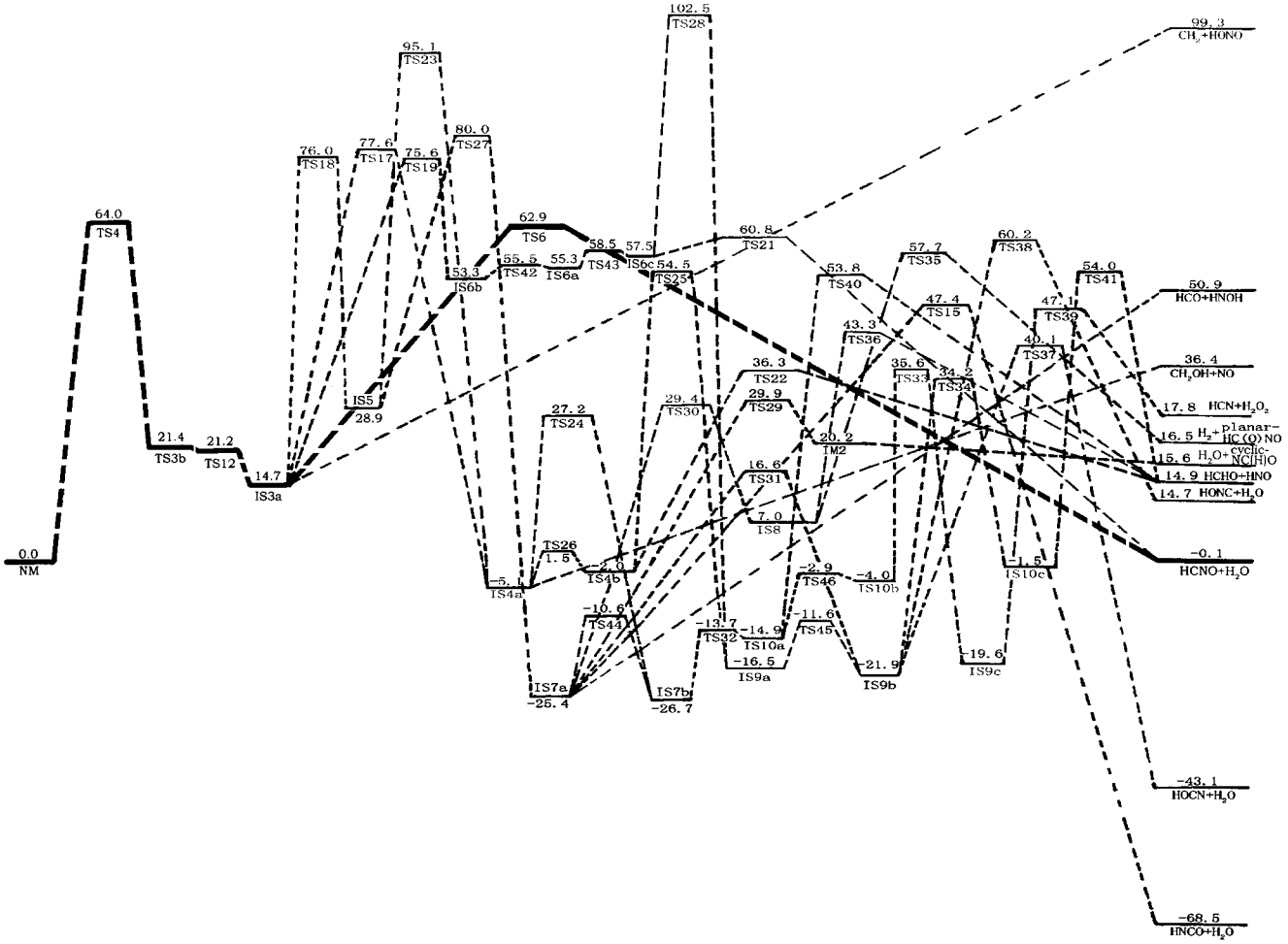

Figure 3. G2MP2 potential energy diagram for CH_3NO_3. Decomposition pathways E. The most feasible decomposition routes are delineated in bold lines. The energies are in kcal/mol.

experimental data indicating the existence of such a loose transition state. In this work, a tight transition state, TS1, is found at the respective C−N and C−O distances of 1.984 and 2.029 Å. IRC calculation confirms the transformation from the staggered NM, IS1b, to the trans-eclipsed methyl nitrite, IS2b, via TS1. At the G2MP2 level, the isomerization barrier is 64.6 kcal/mol (relative to NM), about 2.7 kcal/mol higher than our calculated C−N BDE. By comparison, TS1 is closer to the result by Mckee than to the PES3 by Rice and Thompson, since PES3 is structurally more similar to CH_3ONO than to CH_3NO_2; in that model, the C−N distance is 2.196 Å, whereas the C−O distance is 1.950 Å. This is contrary to our results.

IS1 → IS3 Isomerization. Starting at the staggered CH_3NO_2, IS1b, the rearrangement proceeds through a 1,3-H* transference from carbon to O* atom to arrive at $CH_2N(O)OH$, IS3b. A four-membered ring transition state, TS4, 64.0 kcal/mol above NM, in which the C−H* bond stretches to 1.473 Å and the O*−H* distance diminishes to 1.250 Å, is located for the process.

IS3 → IS4 Isomerization. The rearrangement between $CH_2N(O)OH$ and $CH_2(OH)NO$ occurs via a 1,2-hydroxyl shift from nitrogen atom to carbon. The saddle point, TS17, is found at a N−O distance of 1.961 Å and is confirmed by IRC calculation to connect the planar *cis*-$CH_2N(O)OH$, IS3a to *cis*,*cis*-$CH_2(OH)NO$, IS4a, 19.8 kcal/mol below IS3a. The activation barrier is 62.9 kcal/mol relative to IS3a.

IS3 → IS5 Isomerization. When the O* atom of IS3a transfers instead toward carbon, another isomer, *N*-hydroxyoxaziridene, IS5, in which the C, O*, and N atoms form a three-membered ring, is reached. The process is predicted to be 14.2 kcal/mol endothermic. The transition state TS18, 61.3 kcal/mol above IS3a, is found at a N−O* distance of 1.425 Å, indicating that the unpaired p electron of O* is freed from the resonance structure of IS3a and likely to bond with the unpaired electron of carbon to form CO*N ring.

IS3 → IS6 Isomerization. $CH_2N(O)OH$ isomerization to $HCN(OH)_2$ is made possible by carbonic H* atom of IS3a shifting onto O* via a four-membered ring transition state TS19, 60.9 kcal/mol above IS3a. IS3a can be viewed as a combination of two resonance structures. In one resonance structure (labeled (i) in Figure 1), there are negative charges accumulating on O*. The carbonic H* atom, which is close to O* and carries positive charges, might be drawn toward O* to form the isomer IS6b, 38.6 kcal/mol above IS3a.

IS4 → trans-IS9 Isomerization. The conversion from $CH_2(OH)NO$ to the trans conformer of HC(OH)NOH, IS9a, is made possible by the carbonic H* atom of IS4b shifting onto O* via the four-membered ring transition state TS25, in which the C−H* and O*−H* distances are 1.455 and 1.359 Å, respectively. The isomerization barrier is 56.5 kcal/mol relative to IS4b, and IS9a is energetically 14.5 kcal/mol below IS4b.

IS5 → IS4 Isomerization. The conversion from $H_2(CON)OH$ to $CH_2(OH)NO$ occurs when the hydroxyl H atom shifts onto O* and the N−O* bond in the CO*N ring breaks at the same time. The transition state TS23, 66.2 kcal/mol above IS5 at the G2MP2 level, is found at the O−H distance of 1.031 Å and

the O*CN angle of 96.9°. The process is predicted to be 34.0 kcal/mol exothermic.

IS5 → IS7 Isomerization. When the carbonic H* atom in H_2-(CON)OH transfers instead toward nitrogen atom, the N−O* bond in the CO*N ring will also break to arrive at another isomer HC(O)N(H)OH, IS7a, 54.3 kcal/mol below IS5. The transition state TS27, in which the C−H* bond lengthens to 1.143 Å and the O*CN angle increases to 111.7°, locates 51.1 kcal/mol above IS5.

IS6 → trans-IS9 Isomerization. The direct 1,2-hydroxyl (OH) shift from N to C in the C_1 symmetrical $HCN(OH)_2$, IS6c, may arrive at IS9a. The isomerization transition state TS28, 45.0 kcal/mol above IS6c, is found at the respective N−OH and C−OH distances of 1.487 and 2.042 Å. A considerable energy release, 74.0 kcal/mol, is found for the process.

IS7 → IS4 Isomerization. The electrophilic attack of the hydroxyl H atom toward O* in IS7b, followed by a 1,2-H* shift from nitrogen atom to carbon, may arrive at the *cis,cis*-CH_2-(OH)NO, IS4a, 21.6 kcal/mol above IS7b. The transition state TS24, 53.9 kcal/mol above IS7b, is found at the respective O−H and N−H* distances of 1.786 and 1.289 Å.

IS7 → trans-IS9 Isomerization. HC(O)N(H)OH → HC(OH)-NOH rearrangement occurs when the H atom on N of IS7a transfers onto O* to form the O*−H bond in IS9b, 3.5 kcal/mol above IS7a. The saddle point, TS31, found at the N−H and O*−H distances of 1.324 and 1.361 Å, is 42.0 kcal/mol higher in energy than IS7a.

IS8 → IS7 Isomerization. The N → O coordination bond in $HC(O)N(O)H_2$, IS8, renders O the negative charge center of the H*N(H)O moiety and liable to electrophilic attack by H* atom to reach HC(O)N(H)OH, IS7a, 32.4 kcal/mol below IS8. The transition state TS30, 22.4 kcal/mol above IS8, is found at the respective N−H* and O−H* distances of 1.103 and 1.340 Å.

IS10 → IS7 Isomerization. HC(OH)N(O)H → HC(O)N(H)-OH rearrangement starts at the cis conformer of HC(OH)N-(O)H, IS10a, in which there are negative charges accumulating on O because of the resonance effect of the HC(OH)N(O)H structure. Then the hydroxyl H atom transfers onto O through a five-membered ring transition state, TS32, only 1.2 kcal/mol above IS10a. Finally the reaction system arrives at HC(O)N-(H)OH, IS7b. The process is predicted to be 11.8 kcal/mol exothermic.

cis-IS10 → cis-IS9 Isomerization. The isomerization between the cis conformations of HC(OH)N(O)H and HC(OH)NOH is realized by H* electrophilic attack on O in IS10b to form the O−H* bond of IS9c, 15.6 kcal/mol below IS10b. The transition state TS33, 39.6 kcal/mol above IS10b, is found at the respective N−H* and O−H* distances of 1.117 and 1.307 Å.

trans-IS10 → trans-IS9 Isomerization. The rearrangement between the trans conformers of HC(OH)N(O)H and HC(OH)-NOH occurs via the same mechanism as in the isomerization of their cis conformers, i.e., H* electrophilic attack on O in IS10c to form the O−H* bond of IS9b, 20.4 kcal/mol below IS10c. The isomerization barrier, imposed by TS34, is 35.7 kcal/mol relative to IS10c.

3.2. NM Unimolecular Decomposition Pathways. *Pathway A.*

$$CH_3NO_2 \longrightarrow {}^2CH_3 + {}^2NO_2$$

The C−N bond rupture to yield a methyl radical and nitrogen dioxide is recognized by many as the main primary process for NM decomposition under both thermal[56] and photo[29] conditions. The ultraviolet adsorption spectrum of NM observes a strong band centered at 198 nm, which is assigned as a $\pi^* \leftarrow \pi$ transition localized on the NO_2 moiety,[57] and a weak band at around 270 nm, which is assigned as a $\pi^* \leftarrow$ n excitation of a nonbonding electron of O.[58] Previous REMPI[34] and molecular beam[31] studies suggested that eq 11 was a major channel of dissociation following NM excitation via the $\pi^* \leftarrow \pi$ transition.

$$CH_3NO_2 + h\nu \rightarrow CH_3 + NO_2(1^2B_2) \rightarrow CH_3 + NO(X^2\Pi) + O(^3P) \quad (11)$$

No transition state is found for the simple C−N bond cleavage. Our calculated C−N BDE for CH_3NO_2 is 61.9 kcal/mol, a little higher than the experimental values of 60.1[59] and 58.5 kcal/mol.[60] For the electronically excited NO_2 to undergo further decomposition to the ground-state NO and O (^{3}P), a total amount of energy of 134.7 kcal/mol (about 213 nm) is required. Therefore a 193 nm photon contains sufficient energy to produce the secondary products in eq 11.[34]

Pathway B.

$$CH_3NO_2 \longrightarrow {}^2CH_2NO_2 + {}^2H$$

The single C−H bond dissociation energy is 103.3 kcal/mol by our calculation, about 4.2 kcal/mol lower than the experimental value.[61] Mckee[23] reported a 91.89 kcal/mol C−H BDE for NM, which is close to the value of 88 kcal/mol for the C−H bond of the methyl group in propene. He explained that the C−H bonds in propene and in NM were expected to be weaker, as compared to the standard C−H BDE of 99 kcal/mol, due to resonance stabilization of the propenyl and nitromethyl radicals. However, both our result and experimental result[61] suggest a much higher C−H BDE for CH_3NO_2. This indicates that in addition to the resonance stabilization of the nitromethyl radical, another important factor that influences C−H bond energy in CH_3NO_2 is the strong electron-drawing capacity of the nitro group, which renders C−H bond homolysis more energy consuming. Therefore, compared to its counterpart in propene, the methyl group in NM is at a disadvantage for H atom elimination. Considering these two factors, a C−H BDE of 103.3 kcal/mol for CH_3NO_2 is reasonable.

Pathway C.

$$CH_3NO_2 \dashrightarrow {}^3O + CH_3NO \xrightarrow{TS7} cis\text{-}CH_2NOH \xrightarrow{TS8} trans\text{-}CH_2NOH \xrightarrow{TS9} HCN + H_2O_2$$

O atom elimination as a minor and even major primary dissociation channel has been suggested in both the photolysis[49] and pyrolysis[38] of NM. The process starts on the singlet surface and decays onto the triplet surface to yield CH_3NO + O (^{3}P). A 94.7 kcal/mol energy increase is determined by our calculation, in good agreement with the 93.3 kcal/mol N−O BDE by Rice and Thompson.[21] Nitrosomethane is thermodynamically unstable with respect to isomerization via TS7 into cis-formaldoxime, 6.6 kcal/mol below CH_3NO, which may further decompose into HCN + H_2O via transition states TS8 and TS9. The energy barriers are 59.4 kcal/mol relative to CH_3NO (TS7), 2.8 kcal/mol relative to *cis*-CH_2NOH (TS8), and 56.4 kcal/mol relative to *trans*-CH_2NOH (TS9), respectively. The formation of hydrogen cyanide from formaldoxime is catalyzed appreciably by nitric oxide,[62] an observed major product in the thermolysis of NM.[38−40] Therefore, N−O bond scission is proposed to occur in the initial stage of NM decomposition to explain the large quantities of hydrogen cyanide formed in the experiment by Mueller.[40]

Pathway D.

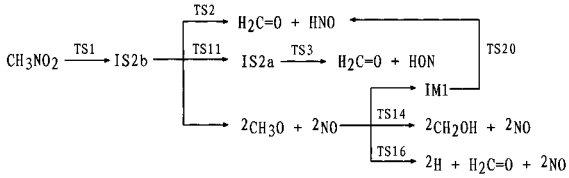

This decomposition pathway proceeds by NM first isomerizing to the trans-eclipsed CH_3ONO, IS2b, via transition state TS1. The nitro-nitrite isomerization barrier is 64.6 kcal/mol, about 2.7 kcal/mol higher than our calculated C−N BDE.

Starting from IS2b, three different reaction paths are explored. The first path is the concerted 1,2-molecular elimination to yield formaldehyde plus nitroxyl, 14.9 kcal/mol above NM.

$$CH_3ONO \rightarrow H_2C{=}O + HNO \qquad (12)$$

The dissociation proceeds through a four-membered ring transition state TS2, in which the breaking O−N and C−H bonds lengthen to 2.075 and 1.366 Å, respectively. The barrier height is 41.0 kcal/mol relative to IS2b.

In the second path, IS2b rearranges first via TS11 into its cis-staggered conformer, IS2a. From IS2a, a concerted 1,3-HON elimination via TS3, 58.1 kcal/mol above IS2a, may occur.

$$CH_3ONO \rightarrow H_2C{=}O + HON \qquad (13)$$

TS3 has the character of a late transition state by its substantially long C−H and O−N bonds (2.262 and 3.115 Å, respectively) and a small imaginary frequency of 78.9 cm^{-1}. In fact, TS3 is so close to the products on the reaction coordinates that the $H_2C{=}O + HON \rightarrow$ IS2a barrier is only 1.9 kcal/mol, indicating that the fragmentation products are kinetically unstable with respect to recombination to the reactant.

The third path is N−O bond rupture in methyl nitrite to yield methanoyl plus nitric oxide, 45.0 kcal/mol above NM. No transition state is located for the process. From the fragments $CH_3O + NO$, three major exit channels are explored. The first one proceeds through transition state TS14, 30.3 kcal/mol above CH_3O, for the $CH_3O \rightarrow CH_2OH$ isomerization. The net energy difference is 8.6 kcal/mol. The second one proceeds through transition state TS16, 22.7 kcal/mol above CH_3O, for the methanoyl C−H bond fission to yield $H + H_2C{=}O + NO$, 62.9 kcal/mol above NM. In the bimolecular step of the third channel, an intermediate IM1, 12.0 kcal/mol above NM, is formed by CH_3O and NO interacting through H and N atoms separated by a distance of 2.326 Å. IM1 then undergoes H atom abstraction from CH_3O by NO via transition state TS20, 31.0 kcal/mol above IM1, to give $H_2C{=}O + HNO$.

Pathway E.

This decomposition pathway starts with NM rearrangement to aci-nitromethane, IS3b, via transition state TS4. The energy barrier, 64.0 kcal/mol at G2MP2 level, is similar to that of NM isomerization to methyl nitrite via TS1, and is 2.1 kcal/mol higher than our calculated C−N bond dissociation energy. IS3b is kinetically rather unstable with respect to conversion to IS3a, which is above NM by 14.7 kcal/mol.

For isomer IS3a, six different reaction channels are explored. The respective IS3a → IS3b, IS3a → IS4a, IS3a → IS5, IS3a → IS6b isomerization barriers via TS12, TS17, TS18, and TS19 are 6.5, 62.9, 61.3, and 60.9 kcal/mol. The activation barrier for the concerted IS3a → $HCNO + H_2O$ elimination via TS6 is 48.2 kcal/mol. No transition state is located for the C−N bond breaking in IS3a, and the IS3a → $CH_2 + HONO$ dissociation energy is 84.6 kcal/mol. It seems that the lowest-energy channel is IS3a → IS3b conversion. However, as we have discussed above, the extremely low IS3b → IS3a barrier renders IS3b kinetically rather unstable for conversion back to IS3a. Hence the lowest-energy exit channel for IS3a is fragmentation to $HCNO + H_2O$, which lies 0.1 kcal/mol below NM. We will then follow the respective IS3a → IS4a, IS3a → IS5, IS3a → IS6b isomerization channels to the formation of final dissociation products.

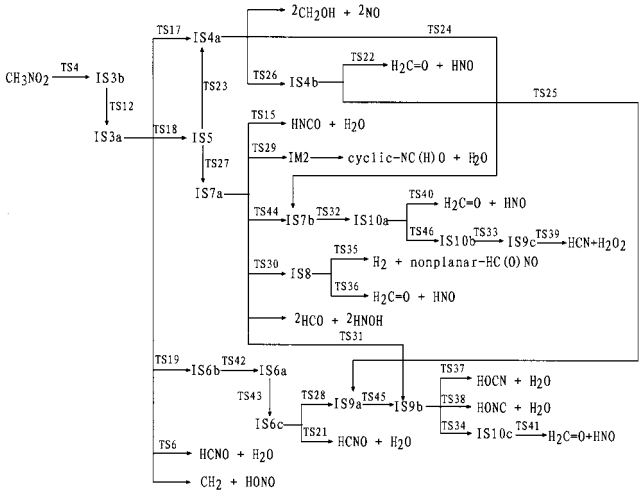

For isomer IS4a, the IS4a → IS3a and IS4a → IS5 isomerization barriers via TS17 and TS23 are forbidding, about 82.7 and 100.2 kcal/mol, respectively. No transition state is found for the C−N bond breaking in IS4a to give the fragments $CH_2OH + NO$, 36.4 kcal/mol above NM. The IS4a → $CH_2OH + NO$ dissociation energy is predicted to be 41.5 kcal/mol. The respective IS4a → IS7b and IS4a → IS4b isomerization barriers via TS24 and TS26 are 32.3 and 6.6 kcal/mol. The exit channels for IS7b may include its conversion into IS7a via TS44, 16.1 kcal/mol above IS7b, and into IS10a via TS32, 13.0 kcal/mol above IS7b. Starting from IS10a, the products $H_2C{=}O + HNO$ may be yielded by overcoming the 68.7 kcal/mol energy barrier imposed by TS40. Or in three consecutive steps, i.e., IS10a → IS10b conversion via TS46, 12.0 kcal/mol above IS10a, followed by IS10b → IS9c isomerization via TS33, 39.6 kcal/mol above IS10b, and the subsequent IS9c → $HCN + H_2O_2$ dissociation via TS39, 66.7 kcal/mol above IS9c, IS10a finally dissociates into $HCN + H_2O_2$, which is 17.8 kcal/mol higher than the NM minimum. The exit channels for IS4b may include the IS4b → IS9a isomerization via TS25, 56.5 kcal/mol above IS4b, and the concerted IS4b → $H_2C{=}O + HNO$ dissociation via TS22, 38.3 kcal/mol above IS4b.

For isomer IS5, the respective IS5 → IS3a, IS5 → IS4a, and IS5 → IS7a isomerization barriers via TS18, TS23, and TS27 are 47.1, 66.2, and 51.1 kcal/mol. Starting at isomer IS7a, seven different reaction channels are explored. The concerted H_2O elimination, IS7a → $HNCO + H_2O$, via TS15 has an energy barrier of 72.8 kcal/mol. The products $HNCO + H_2O$ are energetically 68.5 kcal/mol below NM. IS7a dissociation into cyclic-NC(H)O + H_2O, 15.6 kcal/mol above NM, goes through two consecutive steps, in which IS7a rearranges first to intermediate IM2, 20.2 kcal/mol above NM, via TS29, 55.3 kcal/mol above IS7a, then the loose N−O bond (about 1.820 Å) of IM2 breaks stepwise to give the fragments cyclic-NC(H)O + H_2O. Note that IM2 is energetically 4.6 kcal/mol higher than the fragments by G2MP2 calculation. No transition state is found for the direct C−N bond rupture in IS7a, and the IS7a → HCO + HNOH bond dissociation energy is predicted to be 76.3 kcal/

mol. The respective IS7a → IS5, IS7a → IS7b, IS7a → IS9b, and IS7a → IS8 isomerization barriers via TS27, TS44, TS31, and TS30 are 105.4, 14.8, 42.0, and 54.8 kcal/mol. The exit channels for IS8 may include two concerted molecular eliminations, i.e., IS8 → HC(O)NO + H_2 via TS35, 50.7 kcal/mol above IS8, and IS8 → H_2C═O + HNO via TS36, 36.3 kcal/mol above IS8. The products planar HC(O)NO + H_2 are 16.5 kcal/mol above NM.

For isomer IS6b, the respective IS6b → IS3a and IS6b → IS6a isomerization barriers via TS19 and TS42 are 22.3 and 2.2 kcal/mol. The interconversion among the three conformers of $HCN(OH)_2$, IS6b, IS6a, and IS6c, is comparatively easy considering the low IS6b → IS6a, IS6a → IS6b, IS6a → IS6c, and IS6c → IS6a barriers, as we have discussed above. Starting from IS6c, two exit channels are explored. The energy barrier for the concerted IS6c → HCNO + H_2O dissociation via TS21 is 3.3 kcal/mol. The barrier height for IS6c → IS9a isomerization via TS28 is 45.0 kcal/mol. For isomer IS9a, the respective IS9a → IS6c, IS9a → IS4b, and IS9a → IS9b isomerization barriers via TS28, TS25, and TS45 are 119.0, 71.0, and 4.9 kcal/mol. The exit channels for IS9b include the concerted IS9b → HOCN + H_2O and IS9b → HONC + H_2O dissociations via TS37, 62.0 kcal/mol above IS9b, and TS38, 82.1 kcal/mol above IS9b, as well as the IS9b → IS7a and IS9b → IS10c isomerizations via TS31, 38.5 kcal/mol above IS9b, and TS34, 56.1 kcal/mol above IS9b. The further decomposition of IS10c via the three-membered ring transition state TS41, 55.5 kcal/mol above IS10c, may yield H_2C═O + HNO.

Pathway F.

$$CH_3NO_2 \xrightarrow{TS5} H_2 + HCNO_2 \xrightarrow{TS10} \text{nonplanar-HC(O)NO} \xrightarrow{TS13} \text{planar-HC(O)NO}$$

The activation barrier to NM 1,1-H_2 elimination is extremely high, about 102.2 kcal/mol. This is likely due to the strong electron-drawing capacity of the nitro group in NM, since C−H bond homolysis destroys the donor−acceptor balance established between CH_3 and NO_2 groups. Transition state TS5 is found at the long C−H distances of 1.669 and 1.988 Å. IRC calculations are done on both the forward and reverse directions and locate the staggered NM and H_2 + $HCNO_2$, 96.6 kcal/mol above NM, as the reactant and products.

The $HCNO_2$ structure is characterized by an asymmetrical NO_2 group, in which O* is much closer to carbon than O is. $HCNO_2$ may transform further into the nonplanar HC(O)NO through 1,2-O* shift via TS10, in which the C−O* distance diminishes to 1.640 Å. TS10 is found energetically very close to $HCNO_2$, indicating that $HCNO_2$ is kinetically rather unstable with respect to isomerization into HC(O)NO.

The nonplanar HC(O)NO is further stabilized by conversion to its planar conformer via TS13. Again, TS13 is found very close to nonplanar HC(O)NO in energy. The final products H_2 + planar HC(O)NO are located 16.5 kcal/mol above NM.

3.3. Reaction Mechanism on NM Unimolecular Decomposition PES. In the preceding section, six distinct dissociation pathways of NM have been explored at the G2MP2 theory level. Approximately 16 major dissociation products are formed in the processes. The G2MP2 relative energies of these products are shown as follows: $^2CH_3$ + $^2NO_2$ (61.9 kcal/mol), ^2H + $^2CH_2NO_2$ (103.3 kcal/mol), ^3O + CH_3NO (94.7 kcal/mol), H_2C═O + HNO (14.9 kcal/mol), H_2C═O + HON (57.4 kcal/mol), $^2CH_3O$ + ^2NO (45.0 kcal/mol), $^2CH_2OH$ + ^2NO (36.4 kcal/mol), HCNO + H_2O (−0.1 kcal/mol), HOCN + H_2O (−43.1 kcal/mol), HNCO + H_2O (−68.5 kcal/mol), HONC + H_2O (14.7 kcal/mol), cyclic NC(H)O + H_2O (15.6 kcal/mol), H_2 + planar HC(O)NO (16.5 kcal/mol), HCN + H_2O_2 (17.8 kcal/mol), ^2HCO + ^2HNOH (50.9 kcal/mol), CH_2 + HONO (99.3 kcal/mol).

The schematic profile of the G2MP2 potential energy surface for NM decomposition is plotted in Figures 2 and 3. From the PES presented, we can obtain 11 possible paths that lead to the formation of H_2C═O + HNO as follows.

Path 1: $\text{NM} \xrightarrow{TS1} \text{IS2b} \xrightarrow{TS2} H_2C{=}O + \text{HNO}$

Path 2: $\text{NM} \xrightarrow{TS1} \text{IS2b} \rightarrow CH_3O + \text{NO} \rightarrow \text{IM1} \xrightarrow{TS20} H_2C{=}O + \text{HNO}$

Path 3: $\text{NM} \xrightarrow{TS4} \text{IS3b} \xrightarrow{TS12} \text{IS3a} \xrightarrow{TS17} \text{IS4a} \xrightarrow{TS24} \text{IS7b} \xrightarrow{TS32} \text{IS10a} \xrightarrow{TS40} H_2C{=}O + \text{HNO}$

Path 4: $\text{NM} \xrightarrow{TS4} \text{IS3b} \xrightarrow{TS12} \text{IS3a} \xrightarrow{TS17} \text{IS4a} \xrightarrow{TS24} \text{IS7b} \xrightarrow{TS44} \text{IS7a} \xrightarrow{TS30} \text{IS8} \xrightarrow{TS36} H_2C{=}O + \text{HNO}$

Path 5: $\text{NM} \xrightarrow{TS4} \text{IS3b} \xrightarrow{TS12} \text{IS3a} \xrightarrow{TS17} \text{IS4a} \xrightarrow{TS24} \text{IS7b} \xrightarrow{TS44} \text{IS7a} \xrightarrow{TS31} \text{IS9b} \xrightarrow{TS34} \text{IS10c} \xrightarrow{TS41} H_2C{=}O + \text{HNO}$

Path 6: $\text{NM} \xrightarrow{TS4} \text{IS3b} \xrightarrow{TS12} \text{IS3a} \xrightarrow{TS17} \text{IS4a} \xrightarrow{TS26} \text{IS4b} \xrightarrow{TS22} H_2C{=}O + \text{HNO}$

Path 7: $\text{NM} \xrightarrow{TS4} \text{IS3b} \xrightarrow{TS12} \text{IS3a} \xrightarrow{TS17} \text{IS4a} \xrightarrow{TS26} \text{IS4b} \xrightarrow{TS25} \text{IS9a} \xrightarrow{TS45} \text{IS9b} \xrightarrow{TS34} \text{IS10c} \xrightarrow{TS41} H_2C{=}O + \text{HNO}$

Path 8: $\text{NM} \xrightarrow{TS4} \text{IS3b} \xrightarrow{TS12} \text{IS3a} \xrightarrow{TS18} \text{IS5} \xrightarrow{TS27} \text{IS7a} \xrightarrow{TS30} \text{IS8} \xrightarrow{TS36} H_2C{=}O + \text{HNO}$

Path 9: $\text{NM} \xrightarrow{TS4} \text{IS3b} \xrightarrow{TS12} \text{IS3a} \xrightarrow{TS18} \text{IS5} \xrightarrow{TS27} \text{IS7a} \xrightarrow{TS31} \text{IS9b} \xrightarrow{TS34} \text{IS10c} \xrightarrow{TS41} H_2C{=}O + \text{HNO}$

Path 10: $\text{NM} \xrightarrow{TS4} \text{IS3b} \xrightarrow{TS12} \text{IS3a} \xrightarrow{TS19} \text{IS6b} \xrightarrow{TS42} \text{IS6a} \xrightarrow{TS43} \text{IS6c} \xrightarrow{TS28} \text{IS9a} \xrightarrow{TS25} \text{IS4b} \xrightarrow{TS22} H_2C{=}O + \text{HNO}$

Path 11: $\text{NM} \xrightarrow{TS4} \text{IS3b} \xrightarrow{TS12} \text{IS3a} \xrightarrow{TS19} \text{IS6b} \xrightarrow{TS42} \text{IS6a} \xrightarrow{TS43} \text{IS6c} \xrightarrow{TS28} \text{IS9a} \xrightarrow{TS45} \text{IS9b} \xrightarrow{TS34} \text{IS10c} \xrightarrow{TS41} H_2C{=}O + \text{HNO}$

Among them, the lowest-energy path for H_2C═O + HNO is Path 1, in which the reactant NM rearranges first to IS2b via TS1, followed by IS2b dissociation into H_2C═O + HNO via TS2. The activation barrier is 64.6 kcal/mol imposed by TS1.

In the same way, the lowest-energy path obtained for the formation of H_2C═O + HON is $\text{NM} \xrightarrow{TS1} \text{IS2b} \xrightarrow{TS11} \text{IS2a} \xrightarrow{TS3} H_2C{=}O + \text{HON}$, with an activation barrier of 64.6 kcal/mol (TS1). The lowest-energy path for CH_3O + NO is $\text{NM} \xrightarrow{TS1} \text{IS2b} \rightarrow CH_3O + \text{NO}$, also with a 64.6 kcal/mol energy barrier (TS1). The lowest-energy path for CH_2OH + NO is NM →

IS2b → CH_3O + NO $\xrightarrow{TS14}$ CH_2OH + NO. The highest barrier is 75.3 kcal/mol (TS14 + NO). The lowest-energy path for HCNO + H_2O is NM $\xrightarrow{TS4}$ IS3b $\xrightarrow{TS12}$ IS3a $\xrightarrow{TS6}$ HCNO + H_2O, with a 64.0 kcal/mol barrier (TS4). The lowest-energy path for HOCN + H_2O is NM $\xrightarrow{TS4}$ IS3b $\xrightarrow{TS12}$ IS3a $\xrightarrow{TS17}$ IS4a $\xrightarrow{TS24}$ IS7b $\xrightarrow{TS44}$ IS7a $\xrightarrow{TS31}$ IS9b $\xrightarrow{TS37}$ HOCN + H_2O, with a 77.6 kcal/mol barrier (TS17). The lowest-energy path for HNCO + H_2O is NM $\xrightarrow{TS4}$ IS3b $\xrightarrow{TS12}$ IS3a $\xrightarrow{TS17}$ IS4a $\xrightarrow{TS24}$ IS7b $\xrightarrow{TS44}$ IS7a $\xrightarrow{TS15}$ HNCO + H_2O, also with a 77.6 kcal/mol barrier (TS17). For HONC + H_2O, cyclic-NC(H)O + H_2O, H_2 + planar HC(O)NO, HCN + H_2O_2, and HCO + HNOH, the respective lowest-energy paths are NM $\xrightarrow{TS4}$ IS3b $\xrightarrow{TS12}$ IS3a $\xrightarrow{TS17}$ IS4a $\xrightarrow{TS24}$ IS7b $\xrightarrow{TS44}$ IS7a $\xrightarrow{TS31}$ IS9b $\xrightarrow{TS38}$ HONC + H_2O, NM $\xrightarrow{TS4}$ IS3b $\xrightarrow{TS12}$ IS3a $\xrightarrow{TS17}$ IS4a $\xrightarrow{TS24}$ IS7b $\xrightarrow{TS44}$ IS7a $\xrightarrow{TS29}$ IM2 → cyclic NC(H)O + H_2O, NM $\xrightarrow{TS4}$ IS3b $\xrightarrow{TS12}$ IS3a $\xrightarrow{TS17}$ IS4a $\xrightarrow{TS24}$ IS7b $\xrightarrow{TS44}$ IS7a $\xrightarrow{TS30}$ IS8 $\xrightarrow{TS35}$ H_2 + planar HC(O)NO, NM $\xrightarrow{TS4}$ IS3b $\xrightarrow{TS12}$ IS3a $\xrightarrow{TS17}$ IS4a $\xrightarrow{TS24}$ IS7b $\xrightarrow{TS32}$ IS10a $\xrightarrow{TS46}$ IS10b $\xrightarrow{TS33}$ IS9c $\xrightarrow{TS39}$ HCN + H_2O_2, and NM $\xrightarrow{TS4}$ IS3b $\xrightarrow{TS12}$ IS3a $\xrightarrow{TS17}$ IS4a $\xrightarrow{TS24}$ IS7b $\xrightarrow{TS44}$ IS7a → HCO + HNOH, each with a 77.6 kcal/mol energy barrier (TS17). The path that leads to CH_2 + HONO is NM $\xrightarrow{TS4}$ IS3b $\xrightarrow{TS12}$ IS3a → CH_2 + HONO. The highest energy barrier is 99.3 kcal/mol (IS3a → CH_2 + HONO dissociation), while for the direct NM → CH_3 + NO_2, NM → H + CH_2NO_2, and NM → ^{3}O + CH_3NO bond dissociations, the energy barriers are 64.0, 103.3, and 94.7 kcal/mol, respectively.

From the energetics, it may conclude that the most feasible decomposition pathways for nitromethane are those that lead to CH_3 + NO_2, CH_3O + NO, H_2C=O + HNO, and HCNO + H_2O as follows. Their energy barriers are listed in parentheses.

$$NM \rightarrow CH_3 + NO_2 \text{ (61.9 kcal/mol)}$$

$$NM \xrightarrow{TS1} IS2b \rightarrow CH_3O + NO \text{ (64.6 kcal/mol)}$$

$$NM \xrightarrow{TS1} IS2b \xrightarrow{TS2} H_2C{=}O + HNO \text{ (64.6 kcal/mol)}$$

$$NM \xrightarrow{TS4} IS3b \xrightarrow{TS12} IS3a \xrightarrow{TS6} HCNO + H_2O \quad \text{(64.0 kcal/mol)}$$

For the formation of CH_3O + NO and H_2C=O + HNO, NM isomerization to methyl nitrite via TS1 occurs at the initial reaction stage. Since the concerted IS2b → H_2C=O + HNO dissociation barrier, TS2, is 2.0 kcal/mol lower than the IS2b → CH_3O + NO dissociation energy, the formation of H_2C=O + HNO is energetically favored. For the formation of H_2C=O + HNO and HCNO + H_2O, the two reaction pathways part from each other in the initial step. The former goes through NM → IS2b isomerization, followed by IS2b → H_2C=O + HNO decomposition. The latter proceeds by isomerizing first to aci-nitromethane, which subsequently dissociates into HCNO + H_2O. Considering the very close NM → IS2b and NM → IS3b isomerization barriers, 64.6 and 64.0 kcal/mol, respectively, it seems that the formation of H_2C=O + HNO and HCNO + H_2O may compete with each other. The lowest-energy path for NM decomposition may reside in the formation of CH_3 + NO_2, since our calculated NM → CH_3 + NO_2 bond dissociation energy is 2.7 and 2.1 kcal/mol lower than the respective NM → IS2b and NM → IS3b isomerization barriers.

On the basis of our calculated G2MP2 PES, we have probed qualitatively the possible reaction mechanism of the unimolecular decomposition of NM. Our discussion does not take into account the entropy factor, which also plays an important role in determining the kinetics and thermodynamics of a reaction. In Table 1 we also list the entropies of the relevant isomers, intermediates, transition states, and products obtained at the B3LYP/6-311++G(2d,2p) level. It is shown that the *S* values of the isomers, intermediates, and transition states fluctuate closely around 67 cal mol^{-1} K^{-1}, except for TS3 (78.214 cal mol^{-1} K^{-1}) and TS39 (74.271 cal mol^{-1} K^{-1}). Compared to the generally rather high isomerization and dissociation barrier heights (ΔE) for NM, the influence of the relatively small ΔS values on the rate constants might not be significant. Note that, except for TS3, TS39, and those fragmentation products, the reactant NM has the highest *S* value (71.210 cal mol^{-1} K^{-1}), indicating that the isomers, intermediates, and most transition states are tight compared to NM and disfavored by entropy factor on the Gibbs free energy surface. Certainly those fragmentation products have the highest entropies and will be considerably stabilized with respect to NM on the Gibbs energy profile. Therefore, when entropy is taken into account, the energy profile is not expected to change significantly, except that the isomers, intermediates, and most transition states become slightly destabilized with respect to the reactant, while all fragmentation products are considerably stabilized. And our conclusions will generally not be affected.

4. Conclusions

Six distinct decomposition pathways of nitromethane (NM) are investigated at the G2MP2//B3LYP/6-311++G (2d,2p) theory level. The reaction heats and energy barriers are determined and are in good agreement with the available experimental data. Based on our calculated G2MP2 potential energy surface, the possible NM unimolecular decomposition mechanism is probed. The lowest-energy dissociation channels are shown to be those lead to $^2CH_3$ + $^2NO_2$, $^2CH_3O$ + ^{2}NO, H_2C=O + HNO, and HCNO + H_2O, respectively. Except for HCNO + H_2O, which is energetically very close to NM, all the other three products are thermodynamically less stable than the reactant. The C−N bond dissociation energy of NM is calculated to be 61.9 kcal/mol, lower than the NM to methyl nitrite and NM to aci-nitromethane isomerization barriers by 2.7 and 2.1 kcal/mol, respectively. Our results suggest that the NM rearrangement pathways are kinetically disfavored in view of the relatively high activation barriers, in excess of 60 kcal/mol. The NM dissociation occurs either via the C−N bond rupture or via concerted molecular eliminations.

Acknowledgment. This work was supported by the National Natural Science Foundation of China through Grant 29873043 and 20173051.

Supporting Information Available: Figure S1. Geometric Parameters of Relevant Molecules on the CH_3NO_2 Energy Surface at B3LYP/6-311++G(2d,2p) Theory Level. Bond

lengths are in angstroms and bond angles in degrees. This material is available free of charge via the Internet at http://pubs.acs.org.

References and Notes

(1) Dewar, M. J. S.; Ritchie, J. P. *J. Org. Chem.* **1985**, 50, 1031.

(2) Gindulyte, A.; Massa, L.; Huang, L.; Karle, J. *J. Phys. Chem. A* **1999**, *103*, 11040.

(3) Dibble, T. S.; Francisco, J. S. *J. Phys. Chem.* **1994**, *98*(19), 5010.

(4) Mckee, M. L. *Chem. Phys. Lett.* **1989**, *164*(5), 520.

(5) Gonzalez, A. C.; Larson, C. W.; McMillen, D. F.; Golden, D. M. *J. Phys. Chem.* **1985**, *89*, 4809.

(6) Tsang, W.; Robaugh, D.; Mallard, W. G. *J. Phys. Chem.* **1986**, *90*, 5968.

(7) Saxon, R. P. *J. Phys. Chem.* **1989**, *93*, 3130.

(8) Bianco, R.; Hynes, J. T. *J. Phys. Chem. A* **1999**, *103*(20), 3797.

(9) Mowrey, R. C.; Page, M.; Adams, G. F.; Lengsfield, B. H., III. *J. Chem. Phys.* **1990**, *93*(3), 1857.

(10) Wodtke, A. M.; Hintsa, E. J.; Lee, Y. T. *J. Chem. Phys.* **1986**, *84*, 1044. Wodtke, A. M.; Hintsa, E. J.; Lee, Y. T. *J. Phys. Chem.* **1986**, *90*, 3549.

(11) Rockney, B. H.; Grant, E. R. *J. Chem. Phys.* **1983**, *79*, 708.

(12) Cox, A. P.; Waring, S. J. *J. Chem. Soc., Faraday Trans.* **1972**, *2*, 1060.

(13) Sorensen, G. O.; Pederson, T.; Dreizler, H.; Guarnieri, A.; Cox, A. P. *J. Mol. Struct.* **1983**, *97*, 77.

(14) Mckean, D. C.; Watt, R. A. *J. Mol. Spectrosc.* **1976**, *61*, 184.

(15) Trinquecoste, C.; Rey-Lafon, M.; Forel, M. T. *Spectrochim. Acta* **1974**, *30A*, 813.

(16) Glanzer, K.; Troe, J. *Helv. Chim. Acta* **1972**, *55*, Fasc.8, 2884.

(17) Taylor, W. D.; Allston, T. D.; Moscato, M. J.; Fazekas, G. B.; Kozlowski, R.; Takacs, G. A. *Int. J. Chem. Kinet.* **1980**, *XII*, 231.

(18) Honda, K.; Mikuni, H.; Takahasi, M. *Bull. Chem. Soc. Jpn.* **1972**, *45*, 3534.

(19) Rockney, B. H.; Grant, E. R. *J. Chem. Phys.* **1983**, *79*(2), 708.

(20) Kilic, H. S.; Ledingham, K. W. D.; Kosmidis, C.; McCanny, T.; Singhal, R. P.; Wang, S. L.; Smith, D. J.; Langley, A. J.; Shaikh, W. *J. Phys. Chem. A* **1997**, *101*, 817.

(21) Rice, B. M.; Thompson, D. L.; *J. Chem. Phys.* **1990**, *93*(11), 7986 and the references wherein.

(22) Mckee, M. L. *J. Am. Chem. Soc.* **1985**, *107*, 1900.

(23) Mckee, M. L. *J. Am. Chem. Soc.* **1986**, *108*, 5784.

(24) Mckee, M. L. *J. Phys. Chem.* **1989**, *93*, 7365.

(25) Saxon, R. P.; Yoshimine, M. *Can. J. Chem.* **1992**, *70*, 572.

(26) Roszak, S.; Kaufman, J. J. *J. Chem. Phys.* **1991**, *94*(9), 6030.

(27) Manaa, M. R.; Fried, L. E. *J. Phys. Chem. A* **1998**, *102*, 9884.

(28) Loos, K. R.; Wild, U. P.; Gunthard, Hs. H. *Spectrochim. Acta A* **1969**, *25*, 275.

(29) Bielski, B. H. J.; Timmons, R. B. *J. Phys. Chem.* **1964**, *68*, 347. Napier, I. M.; Norrish, R. G. W. *Proc. R. Soc., Ser. A.* **1967**, *299*, 317.

(30) Kwok, H. S.; He, G. Z.; Sparks, R. K.; Lee, Y. T. *Int. J. Chem. Kinet.* **1981,** 13, 1125; Greenblatt, G. D.; Zuckermann, H.; Haas, Y. *Chem. Phys. Lett.* **1986,** 134, 593.

(31) Butler, L. J.; Krajnovich, D.; Lee, Y. T.; Ondrey, G.; Bersohn, R. *J. Chem. Phys.* **1983**, *79*, 1708.

(32) Blais, N. C. *J. Chem. Phys.* **1983**, *79*, 1723.

(33) Lao, K. O.; Jensen, E.; Kash, P. W.; Butler, L. J. *J. Chem. Phys.* **1990**, *93*, 3958.

(34) Moss, D. B.; Trentelman, K. A.; Houston, P. L. *J. Chem. Phys.* **1992**, *96*(1), 237.

(35) Perche, A.; Tricot, J. C.; Lucquin, M. *J. Chem. Res. Synop.* **1979**, 304.

(36) Hsu, D. S. Y.; Lin, M. C. *J. Energ. Mater.* **1985**, *3*, 95.

(37) Zhang, Y. X.; Bauer, S. H. *J. Phys. Chem. B* **1997**, *101*, 8717.

(38) Taylor, H. A.; Vesselovsky, V. V. *J. Phys. Chem.* **1935**, *39*, 1095.

(39) Cottrell, T. L.; Graham, T. E.; Reid, T. J. *Trans. Faraday Soc.* **1951**, *47*, 584.

(40) Mueller, K. H. *J. Am. Chem. Soc.* **1955**, *77*, 3459.

(41) Blais, N. C.; Engelke, R.; Sheffield, S. A. *J. Phys. Chem. A* **1997**, *101*, 8285.

(42) Winey, J. M.; Gupta, Y. M. *J. Phys. Chem. A* **1997**, *101*, 10733.

(43) Gruzdkov, Y. A.; Gupta, Y. M. *J. Phys. Chem. A* **1998**, *102*, 2322.

(44) Politzer, P.; Seminario, J. M.; Zacarias, A. G. *Mol. Phys.* **1996**, *89*(5), 1511.

(45) Hill, J. R.; Moore, D. S.; Schmdit, S. C.; Storm, C. B. *J. Phys. Chem.* **1991**, *95*, 3037; Malewski, G.; Pfeiffer, M.; Reich, P. *J. Mol. Struct.* **1969**, *3*, 419.

(46) Pangilinan, G. I.; Gupta, Y. M. *J. Phys. Chem.* **1994**, *98*, 4522. Constantinou, C. P.; Winey, J. M.; Gupta, Y. M. *J. Phys. Chem.* **1994**, *98*, 7767. Winey, J. M.; Gupta, Y. M. *J. Phys. Chem. B* **1997**, *101*, 9333. Winey, J. M.; Gupta, Y. M. *J. Phys. Chem. B* **1997**, *101*, 10733.

(47) Chabalowski, C.; Hariharan, P. C.; Kaufman, J. J. *Int. J. Quantum Chem.* **1983**, *17*, 643. Kleier, D. A.; Lipton, M. A. *THEOCHEM.* **1984**, *109*, 39.

(48) Christie, M. I.; Gilbert, C.; Voisey, M. A. *J. Chem. Soc.* **1964**, 3137.

(49) Taylor, W. D.; Allston, T. D.; Moscato, M. J.; Fazekas, G. B.; Kozlowski, R.; Takacs, G. A. *Int. J. Chem. Kinet.* **1980**, *12*, 231.

(50) Jursic, B. S. *Int. J. Quantum Chem.* **1997**, *64*, 263.

(51) Becke, A. D. *J. Chem. Phys.* **1993**, *98*, 5648.

(52) Lee, C.; Yang, W.; Parr, R. G. *Phys. Rev.* **1988**, *B37*, 785.

(53) Foresman, J. B.; Frisch, A. *Exploring Chemistry with Electronic Structure Methods*, 2nd edition; Gaussian, Inc.: Pittsburgh, PA, 1995; p 64.

(54) Curtiss, L. A.; Raghavachari, K.; Pople, J. A. *J. Chem. Phys.* **1993**, *98*, 1293.

(55) Frisch, M. J.; Trucks, G. W.; Schlegel, H. B.; Scuseria, G. E.; Robb, M. A.; Cheeseman, J. R.; Zakrzewski, V. G.; Montgomery, J. A., Jr.; Stratmann, R. E.; Burant, J. C.; Dapprich, S.; Millam, J. M.; Daniels, A. D.; Kudin, K. N.; Strain, M. C.; Farkas, O.; Tomasi, J.; Barone, V.; Cossi, M.; Cammi, R.; Mennucci, B.; Pomelli, C.; Adamo, C.; Clifford, S.; Ochterski, J.; Petersson, G. A.; Ayala, P. Y.; Cui, Q.; Morokuma, K.; Salvador, P.; Dannenberg, J. J.; Malick, D. K.; Rabuck, A. D.; Raghavachari, K.; Foresman, J. B.; Cioslowski, J.; Ortiz, J. V.; Baboul, A. G.; Stefanov, B. B.; Liu, G.; Liashenko, A.; Piskorz, P.; Komaromi, I.; Gomperts, R.; Martin, R. L.; Fox, D. J.; Keith, T.; Al-Laham, M. A.; Peng, C. Y.; Nanayakkara, A.; Challacombe, M.; Gill, P. M. W.; Johnson, B.; Chen, W.; Wong, M. W.; Andres, J. L.; Gonzalez, C.; Head-Gordon, M.; Replogle, E. S.; Pople, J. A. *Gaussian 98*, Revision A.10, Gaussian, Inc.: Pittsburgh, PA, 2001.

(56) Crawforth, C. G.; Waddington, D. J. *Trans. Faraday Soc.* **1969**, *65*, 1334. Crawforth, C. G.; Waddington, D. J. *J. Phys. Chem.* **1970**, *74*, 1425.

(57) Flicker, W. M.; Mosher, O. A.; Kuppermann, A. *J. Chem. Phys.* **1980**, *72*, 2788.

(58) Bayliss, N. S.; McRae, E. G. *J. Phys. Chem.* **1954**, *58*, 1006.

(59) Benson, S. W. *Thermochemical Kinetics*; Wiley: New York, 1976.

(60) Batt, L.; Robinson, G. N. *The Chemistry of Amino, Nitroso, and Nitro Compounds and Their Derivatives*; Patai, S., Ed.; Wiley: New York, 1982.

(61) Knobel, Y. K.; Miroshnichenko, E. A.; Lebedev, Y. *Izv. Akad. Nauk. SSSR, Ser. Khim.* **1971**, *20*, 425.

(62) Taylor, H. A.; Bender, H. *J. Chem. Phys.* **1941**, *9*, 761.